applied sciences

MDPI

Article

A Resveratrol Phenylacetamide Derivative Perturbs the Cytoskeleton Dynamics Interfering with the Migration Potential in Breast Cancer

Jessica Ceramella [1], Adele Chimento [1], Domenico Iacopetta [1,*], Arianna De Luca [1], Gabriela Coronel Vargas [2], Camillo Rosano [2], Vincenzo Pezzi [1], Carmela Saturnino [3] and Maria Stefania Sinicropi [1]

[1] Department of Pharmacy, Health and Nutritional Sciences, University of Calabria, 87036 Rende, Italy; jessica.ceramella@unical.it (J.C.); adele.chimento@unical.it (A.C.); ariannadl@hotmail.it (A.D.L.); v.pezzi@unical.it (V.P.); s.sinicropi@unical.it (M.S.S.)

[2] U.O. Proteomica e Spettrometria di Massa, IRCCS Ospedale Policlinico San Martino, Largo R. Benzi 10, 16132 Genova, Italy; gabrielafernanda.coronelvargas@edu.unige.it (G.C.V.); camillo.rosano@hsanmartino.it (C.R.)

[3] Department of Science, University of Basilicata, Viale dell'Ateneo Lucano 10, 85100 Potenza, Italy; carmela.saturnino@unibas.it

* Correspondence: domenico.iacopetta@unical.it; Tel.: +39-0984493200

Abstract: Chemotherapy is commonly used for cancer treatment, however the lack of selectivity on healthy cells and the development of resistance phenomena are the major issues. A better understanding of cancer genetics helped the development of new targeted anticancer treatments, which permit drug delivery with high specificity and lower toxicity. Moreover, the multi-target drug design concept represents the current trend for future drug research and development. Starting from good results previously obtained by our research group on the resveratrol (RSV) phenylacetamide derivative **2**, which displayed an interesting anti-inflammatory and anti-proliferative activity towards the breast cancer cells MCF-7 and MDA-MB-231, we identified other features, as the ability to perturb the cytoskeleton dynamics and interfere with the migration and metastatic processes. In vitro and in silico studies demonstrate that the derivative **2** is a tubulin and actin polymerization inhibitor and an actin depolymerization promotor. In addition, it interferes with the metastatic potential in both the breast cancer cells, inhibiting the in vitro cell migration and decreasing the spheroids number. These promising results demonstrate that the RSV phenylacetamide derivative **2** could be an important starting point in the discovery and development of safer and more efficacy multi-targeted agents.

Keywords: resveratrol derivative; tubulin; actin; migration; invasion; breast cancer; spheroids; docking studies

Citation: Ceramella, J.; Chimento, A.; Iacopetta, D.; De Luca, A.; Coronel Vargas, G.; Rosano, C.; Pezzi, V.; Saturnino, C.; Sinicropi, M.S. A Resveratrol Phenylacetamide Derivative Perturbs the Cytoskeleton Dynamics Interfering with the Migration Potential in Breast Cancer. *Appl. Sci.* **2022**, *12*, 6531. https://doi.org/10.3390/app12136531

Academic Editors: Francesca Silvagno and Laura Porretti

Received: 31 March 2022
Accepted: 24 June 2022
Published: 28 June 2022

1. Introduction

Cancer is a hyperproliferative disease controlled by multiple genes and various cell signaling pathways. In the past, cancer treatment mainly involved the use of high doses of systemic and non-specific chemotherapy drugs [1]. Unfortunately, severe non-selective toxicity and the development of resistance have limited the use of many drugs [2]. Therefore, the pharmacological approaches to this difficult pathology increasingly require targeted and precise strategies [3,4]. The advanced technology and a better understanding of the genetic cancer cell changes have facilitated the development of a new generation of targeted anticancer treatments [5]. Recently, the use of natural compounds as anticancer agents is rapidly gaining popularity [6] because of their effectiveness against different types of cancer and inducing negligible or no toxic effects [7]. Amongst them, RSV is a natural stilbene with interesting antioxidant, anti-inflammatory, cardioprotective, and anticancer properties [8]. RSV can switch multi-resistance in cancer cells, and it is also able to make cancer cells more sensitive to chemotherapeutic compounds when used in combination with traditional

anticancer drugs [9]. Numerous novel analogs of RSV have been prepared with augmented anticancer activity, bioavailability, and pharmacological profile [10–14]. In our previous work [10], we described the anticancer activity of a series of synthetic RSV phenylacetamide analogs, synthetized by some of us [15]. These compounds possess a monosubstituted aromatic ring that mimics the RSV phenolic nucleus and a longer flexible chain that makes them more stable than RSV. Among the studied compounds, the derivative **2** (Figure 1) resulted in being more bioavailable than RSV and was the most active in exerting anti-inflammatory and anti-proliferative effects, without showing cytotoxicity on healthy cells. In particular, this compound triggered cell cycle arrest and apoptosis in the estrogenic receptor-positive (ER+) MCF-7 and triple-negative MDA-MB-231 breast cancer cells.

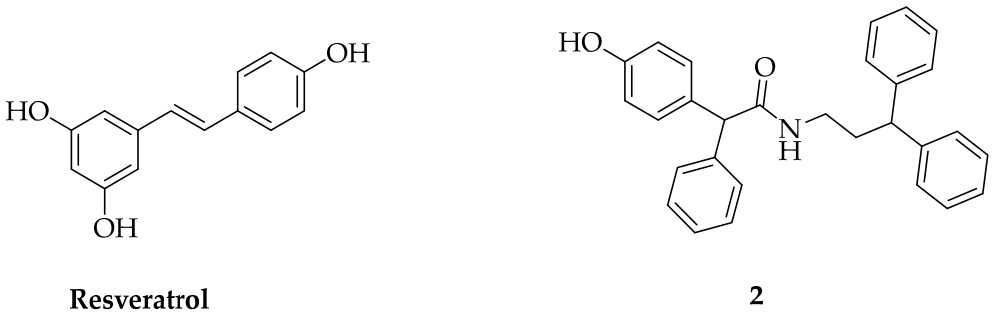

Resveratrol **2**

Figure 1. Molecular structures of Resveratrol and derivative **2**.

Accumulating evidence demonstrates that RSV can interfere with the invasion and migration processes in different tumors via numerous mechanisms and signaling pathways [16]. Thus, in this work, we studied the ability of the most active RSV phenylacetamide (derivative **2**) to interfere with the migration and metastatic processes. During the epithelial–mesenchymal transition (EMT), cancer cells gain migratory and invasive properties that involve a dramatic reorganization of the cytoskeleton components [17]. First, we performed docking studies of derivative **2** on two cytoskeleton major targets, namely tubulin and actin. The obtained results demonstrate that the derivative **2** binds both proteins with high energy and affinity. Then, using immunofluorescence and specific in vitro assays, we confirmed that the derivative **2** effectively acts as a tubulin and actin polymerization inhibitor. In addition, it is also able to accelerate the actin depolymerization, similarly to Latrunculin A, a toxin that causes a rapid disassembly of actin filaments and favors the depolymerization process [18]. Furthermore, the derivative **2** interferes with the metastatic and migratory potential in both the breast cancer MCF-7 and MDA-MB-231 in vitro. Taken together, the obtained results demonstrated that the derivative **2** could represent an interesting new agent useful for the development of safe and effective anticancer drugs targeting cytoskeleton dynamics and blocking the metastatic potential in breast cancer.

2. Materials and Methods

2.1. Cell Cultures

MCF-7 and MDA-MB-231 breast cancer cells and mouse fibroblast 3T3-L1 were purchased from the American Type Culture Collection (ATCC) (Manassas, VA, USA). MCF-7 and MDA-MB-231 breast cancer cells were maintained in Dulbecco's Modified Eagle Medium/F12 (DMEM/F12) supplemented with 5% or 10% fetal bovine serum (FBS) medium respectively, 1% L-glutamine (L-Glu), and 1% penicillin/streptomycin (P/S) (Sigma-Aldrich, Milano, Italy) (complete medium). 3T3-L1 cells were maintained in DMEM with phenol red supplemented with 10% bovine calf serum (BCS), 1% L-Glu, and 1% P/S (complete medium) All cells were maintained at 37 °C in a humidified atmosphere of 95% air and 5% CO_2 and were screened periodically for Mycoplasma contamination. All cell lines were treated in complete medium at the times and concentrations indicated with derivative **2**.

2.2. Docking Studies

The docking simulations were performed using the crystal structures of the Beta/Gamma-Actin with Profilin in complex with the acetyltransferase AnCoA-NAA80 [19] (PDB code 6nbw) and of the tetrameric assembly of Tubulin with Vinblastine (PDB code 5j2t). The molecular structure of the derivative **2** was created and the energy was minimized using the program MarvinSketch (ChemAxon Ltd., Budapest, Hungary). Autodock v.4.2.2. program suite was employed to study the possible binding modes of this compound to both the protein targets and to determine the respective binding energies [20]. In both cases, we performed "blind docking" simulations, as already reported [21–25].

Figures were obtained using the program Chimera [26].

2.3. Immunofluorescence Analysis

Cells were plated in 48-well culture plates equipped with glass slides and exposed to the derivative **2** or RSV for 24 h at the concentration of 25 μM, following a previously described protocol [27]. The primary antibodies used were mouse anti-β-tubulin and mouse anti-β-actin (Santa Cruz Biotechnology, Dallas, TX, USA). The secondary antibody used was Alexa Fluor® 568 conjugate goat-anti-mouse (Thermo Fisher Scientific, Waltham, MA, USA). A fluorescence microscope was employed to acquire the images (Leica DM 6000, Buccinasco, Italy; 40× magnification). LAS-X software was utilized to analyze all the images, which are representative of three separate experiments.

2.4. Tubulin Polymerization Assay

The capability of derivative **2** to interfere with tubulin polymerization was assessed using in vitro Tubulin Polymerization Assay Kit (EMD Millipore Corporation, Burlington, MA, USA), as already described [27]. Briefly, pure bovine tubulin was incubated in a 96-well plate with the test substances, Paclitaxel, Vinblastine, Nocodazole (used as control), and derivative **2**, dissolved in DMSO and used at 10 μM. The turbidity variation was recorded every 30 s at 350 nm for 90 min into the spectrophotometer [27]. Images are representative of three separate experiments, each performed in triplicate and the standard deviations (SD) are reported.

2.5. Actin Polymerization/Depolymerization Assay

Actin Polymerization/Depolymerization Assay Kit purchased from Abcam was used to evaluate the ability of the derivative **2** to interfere with the actin polymerization and depolymerization reaction, as already reported [28]. Latrunculin A and Cytochalasin B were used as control molecules at 5 μM. Derivative **2** was used at 10 μM. The actin filaments assembly was measured by determining the fluorescence ($\lambda_{Ex/Em}$: 365/410 nm) in kinetic mode for 1 h at room temperature using a microplate reader. Images are representative of three separate experiments, each performed in triplicate and the standard deviations (SD) are reported.

2.6. Boyden Chamber Assay

The transwell inserts (8 μm pore size, 24-well plate, Corning Costar, Cambridge, MA, USA) were used to evaluate cell migration ability [29]. The cells (1×10^5/well for MCF-7, 2×10^4/well for MDA-MB-231) were plated in the Boyden insert and vehicle (DMSO) (Sigma-Aldrich, Milano, Italy) or derivative **2** and RSV (20 μM) were added in the well. Cells were allowed to migrate across the membrane for 24 h. At the end of the experiment, the cells were stained with Coomassie Brilliant Blue Solution containing methanol (Sigma-Aldrich, Milano, Italy) for 10 min, and those that did not migrate through the filter were removed from the upper surface of the membrane using cotton-tipped swabs. The migrated cells have been counted under an inverted phase-contrast microscope (Olympus CKX53).

2.7. Wound Healing Assay

MCF-7 and MDA-MB-231 cells were cultured in 12-well plates until approximately 90–100% confluence was achieved; then a sharp edge scratch/wound was made on the cell monolayer using a 10 µL tip. After washing with phosphate-buffered saline (PBS) (Sigma-Aldrich, Milano, Italy) cells were untreated (CTRL) or treated with derivative 2 and RSV (20 µM). Cells were then stained with Coomassie Brilliant Blue solution containing methanol and observed at 0 h and 24 h after scratching by using an inverted phase-contrast microscope (Olympus CKX53). The images are representative of three independent experiments. The wound surface areas were measured using Image J software as previously described [30]

2.8. Three-Dimensional (3D) Spheroids Cultures

A single suspension of MCF-7 and MDA-MB-231 cells was prepared using 1X Trypsin-EDTA (ethylenediaminetetraacetic acid) solution (Sigma-Aldrich) and manual disaggregation (21 gauge needle) [31]. Cells were seeded in non-adherent conditions as previously described [32].

2.9. Statistical Analysis

All experiments were performed at least three times. Data represent the mean values ± standard deviation (SD). The GraphPad Prism 5.0 software (GraphPad Software, Inc., San Diego, CA, USA) was used to calculate the statistical significance between untreated (CTRL) and treated samples. Untreated and treated samples were compared using the analysis of variance (ANOVA) with Bonferroni or Dunn's post hoc testing. Significance was defined as $p < 0.05$.

3. Results and Discussion

3.1. Docking Studies

Considering the several pieces of evidence establishing that RSV is able to inhibit the invasion and migration events in different tumors, which involve dramatic reorganization of the cytoskeleton components [16], first, we performed docking studies of RSV derivative **2** on two cytoskeleton major targets, namely tubulin and actin. We initially analyzed the binding of derivative **2** with tubulin by performing docking simulations using the 3D structure of tubulin as the protein target. Binding energies of the complex formed by the compound and the protein were calculated by Autodock, and their affinity was obtained using the expression Ki = exp (deltaG/(R*T)). As already reported by us [33–35], the outcomes from our simulation runs were clusterized and the analysis of the clusters and the visual inspection of the ligand:protein binding site were considered a marker for the quality of the interaction.

In this specific case, the derivative **2** binds, with good energy (−9.02 kCal/mole), the interface formed between the subunits α and β of the tubulin tetrameric assembly, in correspondence with the binding site of Vinblastine (Figure 2). In particular, this compound forms hydrogen bonds with residues Glu α254, Asp β179, Tyr β224, and hydrophobic interactions with amino acids Leu α248, Pro α25, Val α328, Val α353, and Tyr β210, Pro β222, Tyr β224. Our compound is fully superposed to the binding site of Vinblastine, thus we can assess that the derivative **2** can inhibit the regular polymerization process of tubulin.

Then, we analyzed the binding of the derivative **2** to actin using the three-dimensional structure of actin as the protein target [19]. The derivative **2** also binds with a good energy (−7.36 kcal/Mole) to a cleft in the proximity of the Profilin binding area (Figure 3). This compound, therefore, could favor and stabilize the formation of Actin:profilin complex, hampering the correct mechanism of cellular remodeling and plasticity [36]. In deeper detail, the derivative **2** creates hydrogen bonds with actin residues Arg 116 and His 371 and with Profilin residues Arg 74, Asn124, and Lys 125. This binding is further stabilized by hydrophobic interactions with residues Pro 109, Leu 110, Pro 112, Ile 136, Tyr 169, Pro 172,

and a π-π stacking with Phe 375 belonging to actin and with Ile 73 and Tyr 128 belonging to Profilin.

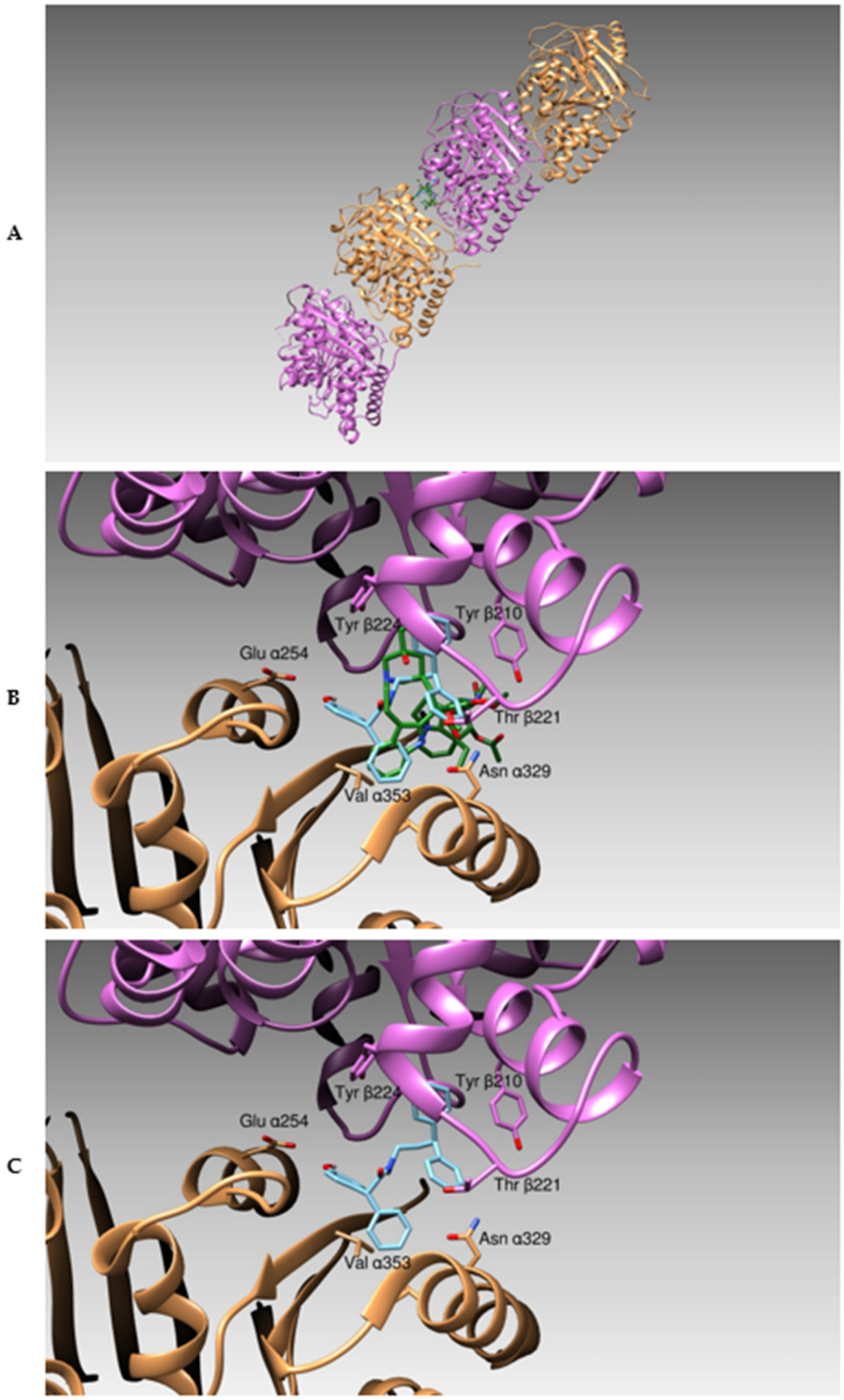

Figure 2. (**A**) Tetrameric alpha-beta-alpha-beta (alpha represented as salmon ribbons, beta as purple ribbons) tubulin assembly. The binding site of derivative **2** (cyan sticks) is located at the interface between beta and alpha subunits, in correspondence to the Vinblastine binding site (highlighted as green sticks). (**B**) Reports the superposition of the Vinblastine (green) binding site (as determined by X-ray Crystallography) to that of the derivative **2** (cyan), as determined by our simulations. (**C**) Reports the interactions between the protein assembly and the derivative **2**.

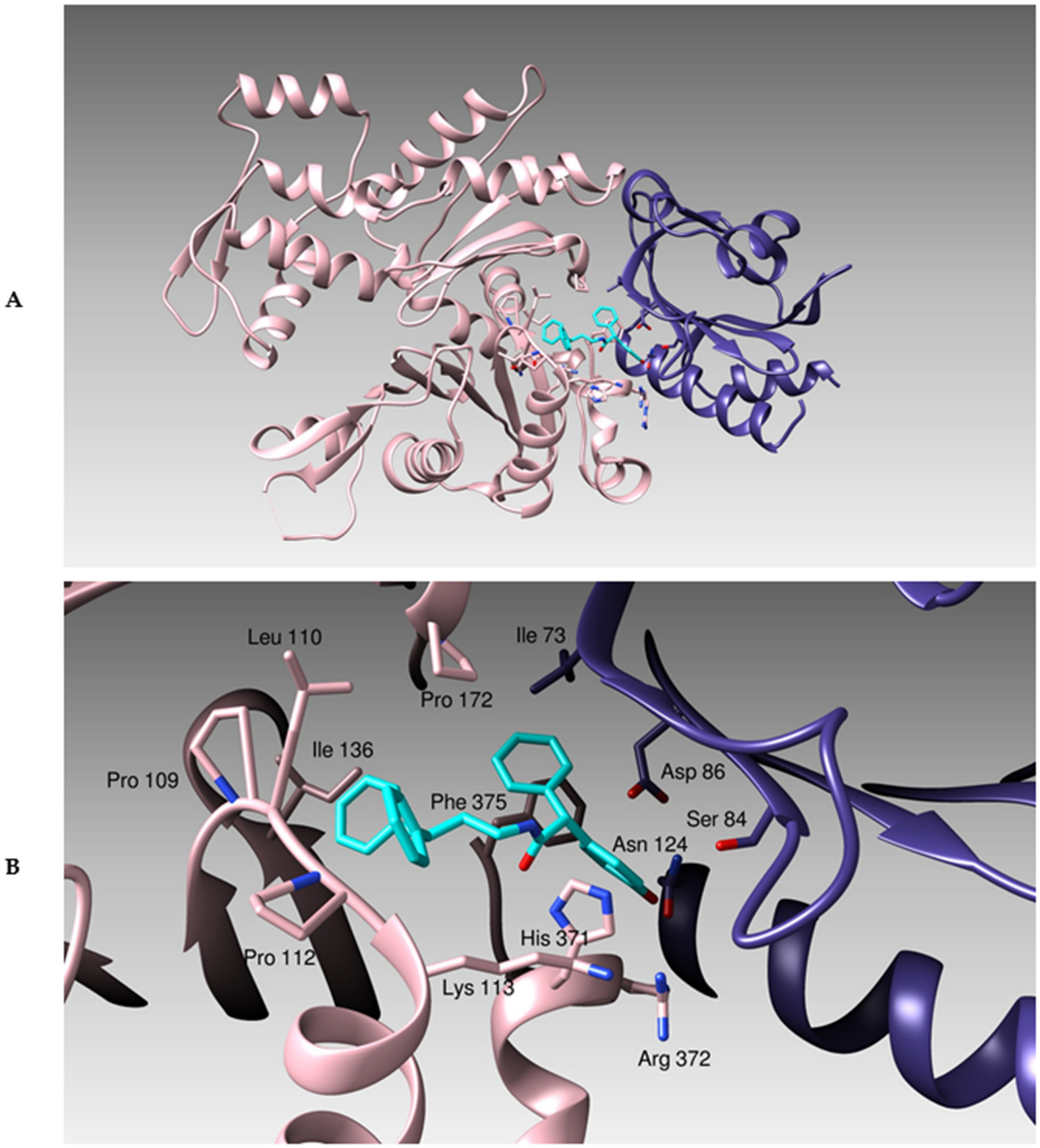

Figure 3. (**A**) A schematic view of the derivative **2** (drawn as cyan sticks) binding site located at the interface between actin (pink ribbons) and profilin (violet ribbons); (**B**) A detailed view of the interface between actin and Profilin allows to identify the different residues involved in the derivative **2** binding.

3.2. The Derivative **2** *Inhibits Tubulin Polymerization*

Microtubules represent an important target in cancer therapy since they play a key role in various cellular functions such as mitosis, cell signaling, and organelle trafficking [37]. Indeed, microtubule-targeting agents, such as vinca alkaloids and taxanes, are successfully used in the clinic for the treatment of different kinds of cancers, but drug resistance onset and high toxicity represent the major issues. Different literature data indicated that some natural compounds, including RSV and some derivatives, exhibit their anticancer activity through the disruption of the microtubule dynamics, interfering with tubulin, without showing the limitations of traditional microtubule-targeting agents [38–40]. In previous

work, we assessed the interesting anticancer activity of the RSV derivative **2** on two breast cancer cell lines, MCF-7 and MDA-MB-231, without showing any cytotoxicity on the healthy cells [10]. Thus, in order to confirm in silico studies, we evaluated its ability to interfere with tubulin using immunofluorescence studies on both breast cancer cells. Figure 4 shows that the treatment with the derivative **2** (25 μM) induced a total microtubule disorganization with tubulin filaments amassed inside the cell cytoplasm, creating the typical crystals, indicated by the white arrows (Figure 4, Panels B, derivative **2**, MCF-7, and MDA-MB-231). Whereas in vehicle-treated cells, tubulin filaments resulted showed that they were well assembled and regularly distributed in the cytoplasm (Panels B, CTRL, MCF-7, and MDA-MB-231). A parallel experiment has been conducted on 3T3-L1 cells, demonstrating that the derivative **2** had no effect on the microtubules of the normal cell (Figure 4, Panels B, derivative **2**, 3T3-L1). Finally, the effect of RSV on the cytoskeleton of all the used cell lines was also assessed. The results demonstrated that MCF-7, MDA-MB-231 and 3T3-L1 cells exposed to RSV showed a regularly organized tubulin cytoskeleton (Figure 4, Panels B, RSV, MCF-7, MDA-MB-231, and 3T3-L1).

In order to assess if the derivative **2** act as stabilizing- or destabilizing-microtubules agents, we also examined its effect on the tubulin polymerization reaction using a specific in vitro assay. We used three reference molecules, two tubulin polymerization inhibitors, Vinblastine and Nocodazole, and a stabilizing agent, Paclitaxel. The turbidity variation linked to the tubulin polymer formation was recorded each 30 s at 350 nm for 3600 s. In Figure 5, it is possible to observe that in the control reaction the tubulin polymerization rapidly occurred, in a time-dependent manner, reaching the plateau phase after 17 min with a maximal optical density (OD350) of 0.49. Paclitaxel caused a more rapid tubulin heterodimer assembly than in the control reaction. The steady-state was reached after less than 15 min with an OD350 of 0.54. The OD350 at 90 min was about 0.41 and 0.44 for control and Paclitaxel, respectively. Whereas, using Vinblastine or Nocodazole, the polymerization reaction was impeded (final OD350 of 0.19 and 0.28, respectively). The derivative **2** (used at the concentration of 10 μM) was also able to inhibit the tubulin polymerization with an effectiveness similar to Nocodazole, but to a lesser extent with respect to Vinblastine, indeed the polymerization curve reached the plateau after 30 min at an OD350 1.4-fold reduced than the control reaction (OD350 = 0.35), with a final OD350 value of about 0.32. Thus, the derivative **2** resulted in a promising in vitro inhibitor of tubulin polymerization.

3.3. Derivative **2** *Interferes with Actin Polymerization and Depolymerization*

A multitarget therapy is considered a successful approach to obtain compounds with higher therapeutic effectiveness and fewer side effects, thus we evaluated whether the derivative **2** could interfere with another important cytoskeleton component, i.e., actin, as already supposed by docking simulations. The actin cytoskeleton is a dynamic network strictly implicated in migration and invasion processes [6], and cancer cells can exploit the actin system to escape from primary tumors and spread to distant organs. Thus, targeting the actin cytoskeleton represents a valid strategy in cancer treatment [7]. For this purpose, MCF-7 and MDA-MB-231 cells were treated for 24 h with the derivative **2** (used at 25 μM) or with vehicle (DMSO, negative control). The IF results, shown in Figure 6, demonstrate that the derivative **2** also interferes with the normal organization of the actin system in both breast cancer cells. Indeed, contrarily to the DMSO-treated cells (CTRL), which showed a normal arrangement of the actin filaments within the cell cytoplasm (Figure 6, Panels B, CTRL, MCF-7, and MDA-MB-231), both the breast cancer cells exposed to the derivative **2** exhibited a strong disorganization of the actin system (Figure 6, Panels B, derivative **2**, MCF-7, and MDA-MB-231). In particular, cancer cells lost their normal morphology, appearing with a smaller size and round. Moreover, the actin system resulted squeezed in a dot-like structure and not well distributed in the cytoplasm and the actin filaments are more stocked around the cell nuclei, appearing also brighter (see white arrows in Figure 6). A parallel experiment has been conducted on the mouse fibroblast 3T3-L1 cells, demonstrating that the derivative **2** had no effect on the actin cytoskeleton of the normal cells (Figure 6,

Panels B, derivative **2**, 3T3-L1). Finally, the effect of RSV on the actin cytoskeleton of all the used cell lines was also assessed. The results demonstrated that MCF-7, MDA-MB-231 and 3T3-L1 cells exposed to RSV showed a regularly organized actin cytoskeleton (Figure 6, Panels B, RSV, MCF-7, MDA-MB-231, and 3T3-L1).

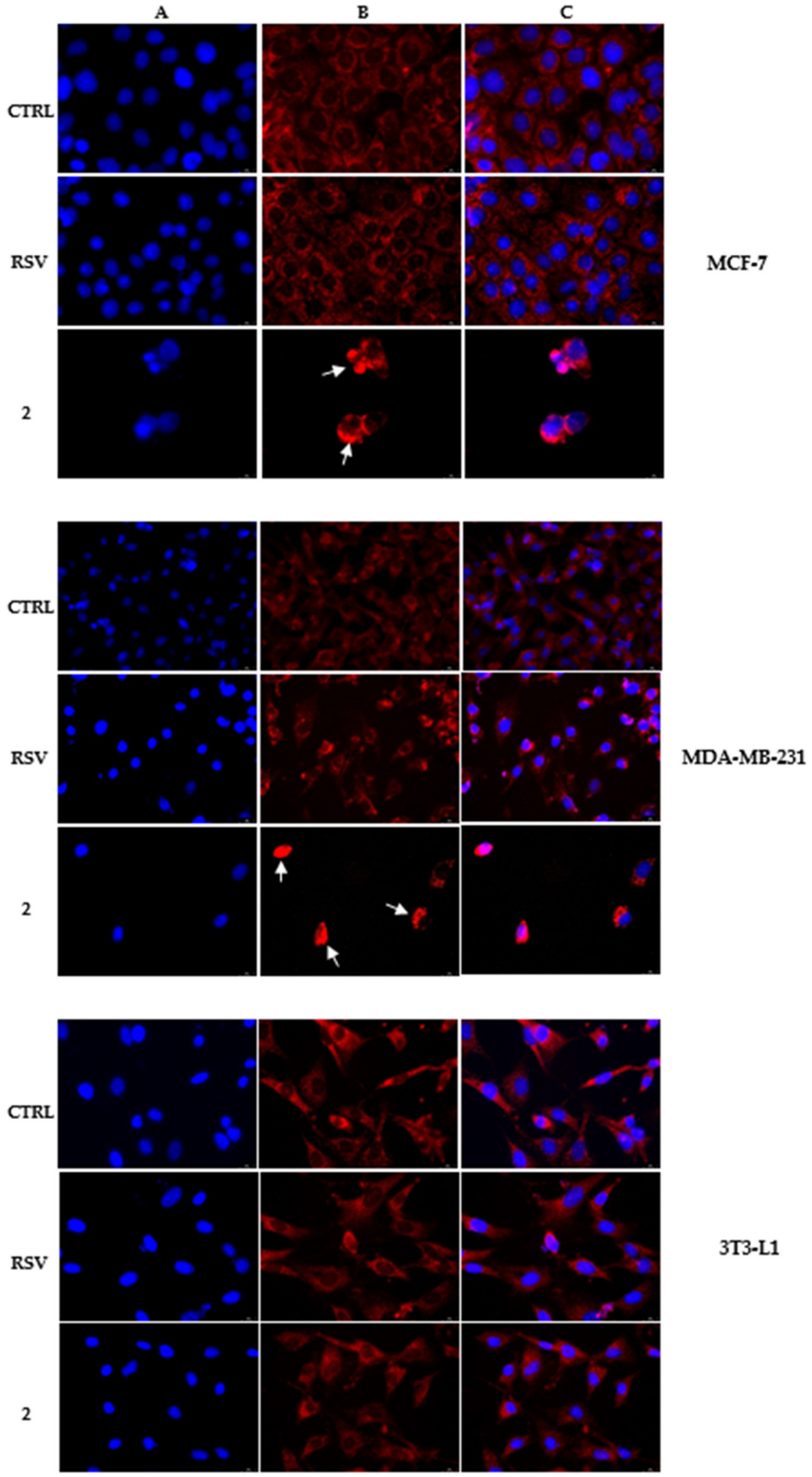

Figure 4. β-Tubulin immunofluorescence studies. MCF-7 and MDA-MB-231 breast cancer cells and

3T3-L1 cells treated with the derivative **2** (25 μM), RSV (25 μM), or with the vehicle (CTRL, DMSO) for 24 h, were incubated with a mouse anti-β-tubulin primary antibody and then with the mouse secondary antibody. CTRL cells and RSV-treated cells showed a regular cytoskeleton organization in all the cell lines used; 3T3-L1 cells treated with the derivative **2** also showed a normal arrangement of tubulin microtubules; contrarily, the derivative **2** induced a strong microtubules disorganization in both the breast cancer cells (see white arrows). Cells were monitored using the inverted fluorescence microscope at 40× magnification. (**A**) DAPI ($\lambda_{ex}/\lambda_{em}$ = 350/460 nm); (**B**) β-tubulin (Alexa Fluor® 568 ($\lambda_{ex}/\lambda_{em}$ = 644/665 nm); (**C**) overlay channel. The images are representative fields.

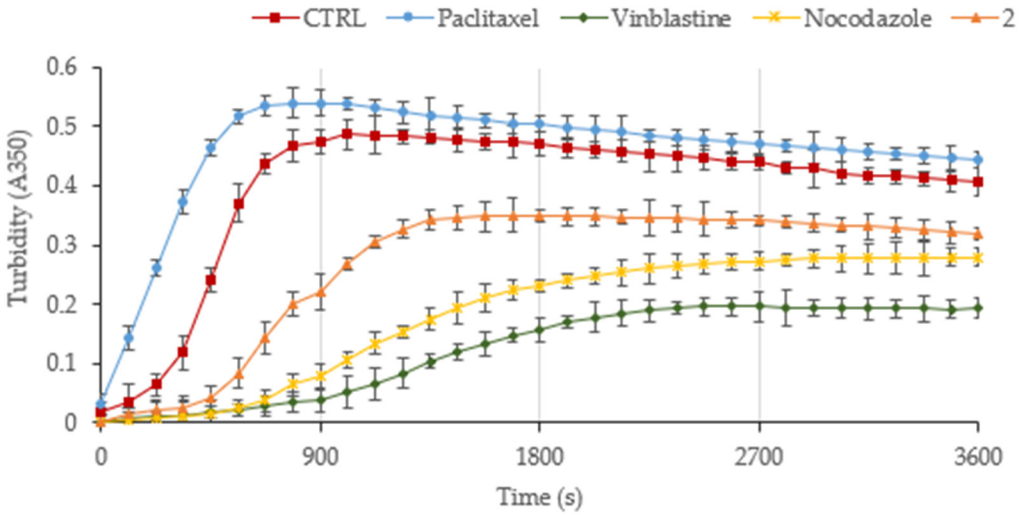

Figure 5. Effects of derivative **2** on tubulin polymerization. The effect of the derivative **2** on in vitro tubulin polymerization was evaluated by recording the turbidity difference at 350 nm for 3600 s (see the experimental section for further details). Paclitaxel was used as a tubulin-stabilizing agent, while Vinblastine and Nocodazole were used as tubulin-destabilizing agents. The three reference molecules and the derivative **2** were tested at the concentration of 10 μM. DMSO was used as a negative control. The graphics are representative of three separated tests; standard deviations (SDs) are shown.

Further, we performed specific in vitro actin polymerization and depolymerization assays, using a fluorescent-labeled rabbit muscle actin reconstituted and Latrunculin A (LA), and Cytochalasin B (CB) as positive controls (5 μM).

In the actin polymerization assay (Figure 7A), the plotted relative fluorescence indicated that the derivative **2** (used at the concentration of 10 μM) strongly impeded the actin polymerization, with a similar effectiveness to LA and CB. Indeed, the control reaction (DMSO) showed a very fast actin polymerization as the reaction curve reached a value of about 25,000 relative fluorescence units (RFU) after 7/8 min, sustaining the plateau until the end. On the contrary, the LA curve, starting from 14,000 RFU, rapidly decreased after 5 min reaching an RFU of 11,000. The fluorescence continued to decline until the end of the experiment, where it reached the value of 8400 RFU. The exposure of the actin monomers to CB produced a curve with a lesser decrease than the LA curve in the first 5 min (about 12,000 RFU), then the curve increased, ending at about 13,300 RFU. The curve obtained after the exposure to the derivative **2** (10 μM) showed, in the initial part, a similar fashion to that of LA. In particular, the curve reached a lower RFU than the LA curve in the first 5 min (10,000 RFU). Then, the two curves superpose from 11 to 30 min, and in the last part, the curve of derivative **2** increased, reaching a final RFU of about 13,500.

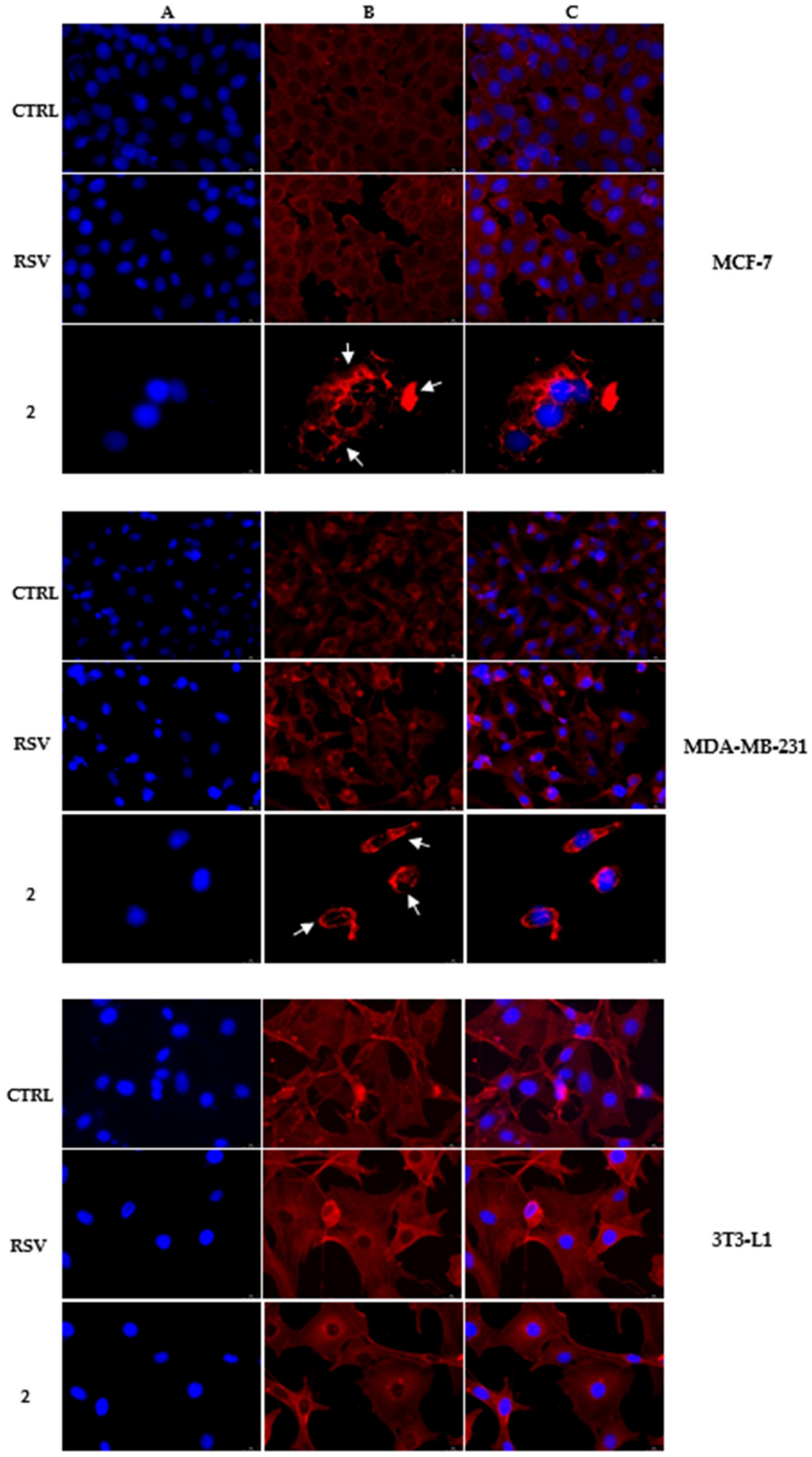

Figure 6. β-Actin immunofluorescence studies. MCF-7 and MDA-MB-231 breast cancer cells and 3T3-L1 cells were exposed to the derivative **2** (25 μM), RSV (25 μM), or with the vehicle (CTRL, DMSO) for 24 h. CTRL cells and RSV-treated cells showed a normal organization of the actin filaments within the cell cytoplasm; 3T3-L1 cells treated with the derivative **2** also showed a normal arrangement of the

actin system; contrarily, both the breast cancer cells exposed to the derivative **2** exhibited a strong disorganization of the actin system. Cells were monitored using the inverted fluorescence microscope at 40× magnification. (**A**) DAPI ($\lambda_{ex}/\lambda_{em}$ = 350/460 nm); (**B**) β-actin (Alexa Fluor® 568 ($\lambda_{ex}/\lambda_{em}$ = 644/665 nm); (**C**) overlay channel. Representative fields are shown.

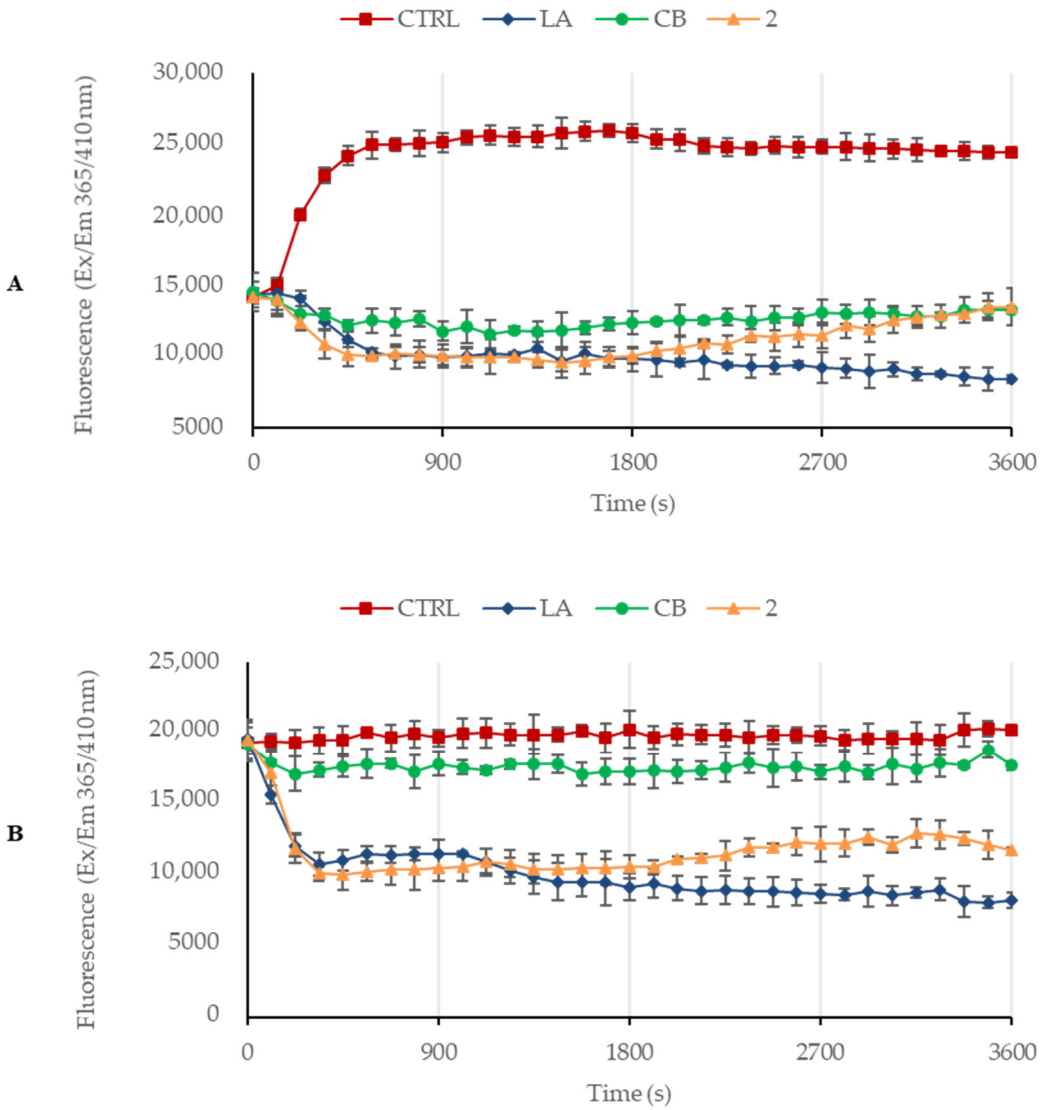

Figure 7. (**A**) In vitro actin polymerization assay and (**B**) in vitro actin depolymerization assay. For both the assays, derivative **2** was used at the concentration of 10 μM, DMSO was used as a negative control, while actin-targeting agents, LA and CB (5 μM), were used as reference molecules. The formation of the actin filaments was measured with a microplate reader recording the fluorescence ($\lambda_{ex/em}$: 365/410 nm) in kinetic mode for 1 h. The graphics are representative of three separated tests; standard deviations (SDs) are shown.

To assess whether the derivative **2** could act also on F-actin disassembly, we performed a depolymerization assay (Figure 7B). First, we allowed the actin polymerization for one hour, and then we added the derivative **2**, in the same experimental condition used for the polymerization assay, monitoring the reactions for another hour. LA was used as a positive control and CB or vehicle (DMSO) were used as negative controls.

In negative controls, the curves maintained the same initial RFU value until the end of the experiment, indicating no F-actin depolymerization.

Instead, the LA curve decreased until a value of 10,000 RFU in the first 5 min (initial value 19,000 RFU), indicating that the actin depolymerization was occurring. Then, after

a small but not significant increase, the curve slowly decreased until the final value of 8000 RFU. The derivative **2** resulted also able to induce the F-actin depolymerization, with a similar effectiveness to LA. Indeed, in the initial part, the derivative **2** curve is to that of LA, reaching an RFU of 10,000 after only 4/5 min and maintaining it until 30 min. In the final part, the curve slowly increased, touching 12,000 RFU at the end of the experiment. Taken together, these outcomes demonstrated that the derivative **2** can inhibit the actin polymerization and, at the same time, induce the formation of actin monomers triggering the F-actin depolymerization, mimicking the LA behavior.

3.4. Derivative **2** *Reduces Motility of Human Breast Cancer Cells*

Dynamic remodeling of filamentous actin under the plasma membrane [41] results in the formation of membrane protrusions such as filopodia, lamellipodia, and invadopodia on the leading edge, which represent critical events for most types of cell migration. It is known that cell migration is an important event, involved in regulating many biological processes in physiological and pathological conditions, such as tumor invasion and metastasis [42]. To examine the effects of derivative **2** on migratory and invasive properties of breast cancer cells, Boyden Chamber (Figure 8A) and wound healing (Figure 8B) assays were performed. Results reported in the figure clearly confirmed that derivative **2,** unlike the RSV, is able to significantly inhibit the migratory potential of both MCF-7 and MDA-MB-231 cells (Figure 8A,B).

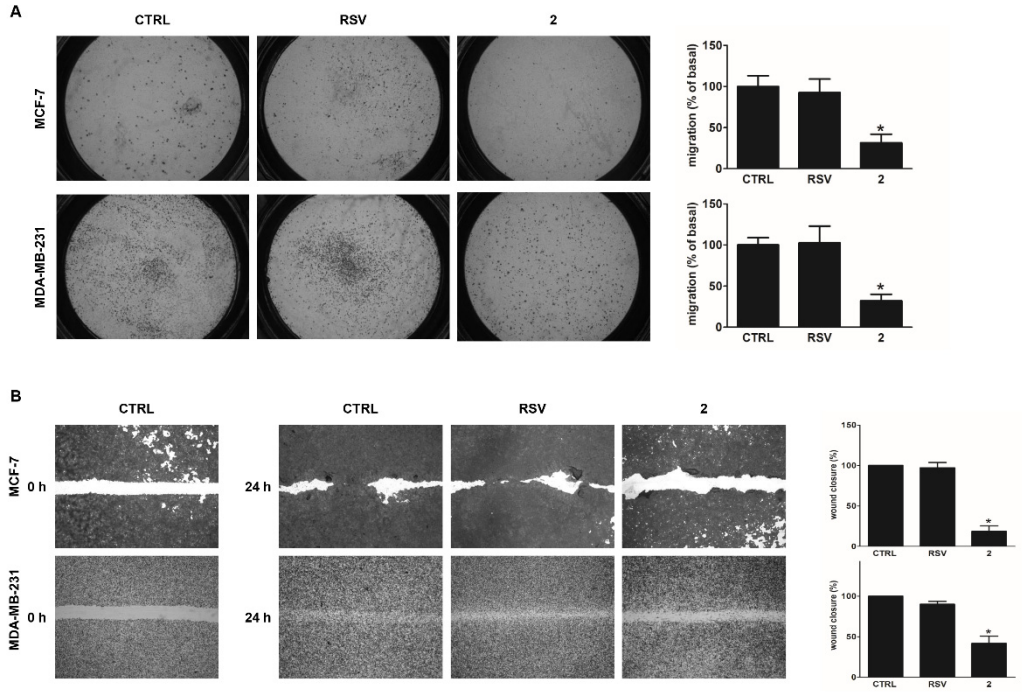

Figure 8. Derivative **2** interferes with breast cancer cell motility. (**A**,**B**) MCF-7 and MDA-MB-231 cells were untreated (CTRL) or treated with derivative **2** (**2**) and RSV (20 μM) for 24 h. Boyden Chamber (**A**) and Wound Healing (**B**) assays were used to evaluate tumor cells' migratory behavior as described in the "Materials and Methods" section. Images are from a representative experiment (**A**,**B**, magnification ×20, scale bar: 500 μm). (**A**) In the Boyden Chamber assay, after adding derivative **2** or RSV in the lower compartment, the migrated cells were observed under an inverted phase-contrast microscope and then counted. The graph represents the mean ± SD of three independent experiments of migrated cells number expressed setting untreated cells as 100% (CTRL) (* $p \leq 0.05$ vs. CTRL). (**B**) The wound is observed immediately (0 h) and 24 h after the scratch. Right graphs represent the quantitative analysis of wound closure. Data represent the mean values ± SD of three independent experiments. (* $p < 0.05$ vs. CTRL).

3.5. Derivative **2** *Decreases Anchorage-Independent 3-D Spheres Formation in Human Breast Cancer Cells*

Cancer metastasis is highly dependent on the formation of three-dimensional spheroids [43]. The main feature of three-dimensional tumor cell cultures is to have an expression pattern of adhesion and extracellular matrix (ECM) molecules, as well as metastasis-related proteins, which is similar to that found within in vivo cancers [44,45]. This model system enriches spheres of cancer stem cells and progenitor cells and more closely mimics tumors in vivo [32]. We then evaluated MCF-7 and MDA-MB-231 breast cancer cells' ability to grow in an anchorage-independent manner forming 3-dimensional spheres. Results demonstrated that when MCF-7 and MDA-MB-231 cells were maintained as spheroids in the presence of derivative **2**, a significant reduction in tumorspheres formation (Figure 9) was observed. Moreover, the use of RSV affects the ability to form tumor spheroids less in both cell lines tested compared to derivative **2** (Figure 9). Altogether, these data suggest that derivative **2** can interfere with metastatic potential in breast cancer.

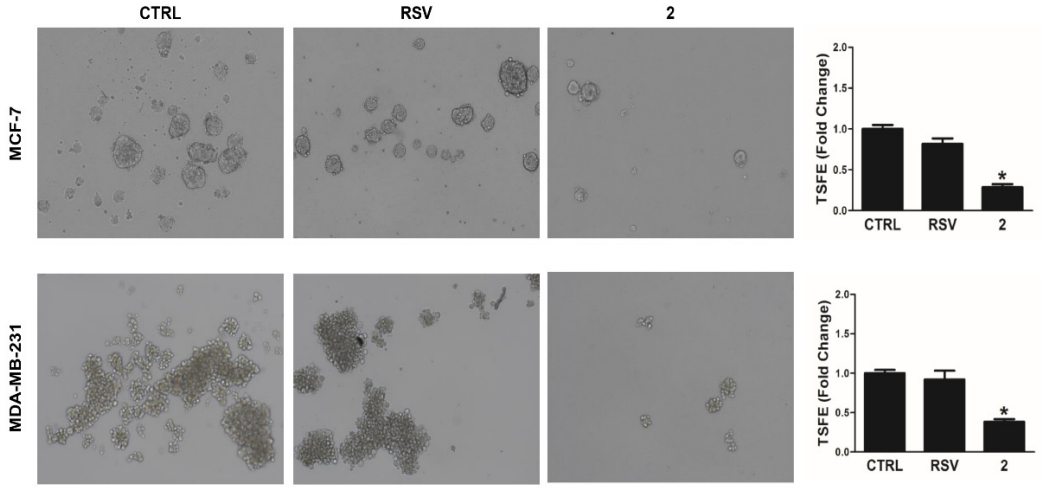

Figure 9. Derivative **2** inhibits breast cancer cell 3D-spheroid formation. MCF-7 and MDA-MB-231 cells were plated on low-attachment plates and then left untreated (CTRL) or treated with derivative **2** (**2**) and RSV (20 μM). Spheroid formation capability of untreated and treated cells was determined in a 3D spheroid assay as described in "Materials and Methods". Tumor spheres formation efficiency (TSFE) was evaluated five days later (* $p < 0.05$ vs. untreated cells). Images are from a representative experiment (magnification ×100, scale bar: 100 μm). Right graphs represent the mean values ± SD of three independent experiments of 3D-spheroids formed and expressed as fold change over untreated cells (CTRL) (* $p < 0.05$ vs. CTRL).

4. Conclusions

Cell migration plays a significant role in physiological conditions, such as embryonic morphogenesis, nervous system development, tissue homeostasis, and immune cell trafficking [46,47], but can be deregulated as well, contributing to several pathological processes such as inflammation and cancer metastasis [48]. Tumor cell migration and invasion involve several events, including remodeling of the cell cytoskeleton, thus the employment of drugs targeting this structure is of notable interest in the pharmaceutical field. Here, we demonstrated that a synthetic derivative of RSV possesses a strong activity on two main proteins forming the cell cytoskeleton, namely tubulin and actin. Particularly, by using in silico and in vitro studies, we discovered that RSV derivative **2** is able to inhibit tubulin and actin polymerization and, most interestingly, induce the F-actin depolymerization, with a common and synergic final effect, i.e., the structural dysfunction of cancer cells cytoskeleton. These exciting features are responsible for the observed reduced metastatic and migration potentials of the breast cancer cells used as models, as demonstrated by wound healing, Boyden Chamber, and 3D-spheroid formation assays. We are confident

that these studies may support and push the research of anticancer drugs, derived from natural products, gifted with synergic multi-target effects and lower toxicity.

Author Contributions: Conceptualization, J.C., A.C. and D.I.; methodology, D.I. and A.C.; software, C.R. and G.C.V.; validation, D.I.; investigation, J.C. and A.D.L.; data curation, C.S. and V.P.; writing—original draft preparation, J.C. and A.C.; writing—review and editing, D.I. and M.S.S.; visualization, V.P. and C.S.; supervision, M.S.S.; funding acquisition, V.P., A.C., A.D.L. and C.R. All authors have read and agreed to the published version of the manuscript.

Funding: This work was supported by a special award (Department of Excellence, Italian Law 232/2016) from the Italian Ministry of Research and University (MIUR) to the Department of Pharmacy, Health and Nutritional Sciences of the University of Calabria (Italy), and by MIUR ex 60% (V.P., A.C.) and by AIRC (Associazione Italiana per la Ricerca sul Cancro), projects n. IG20122. A.D.L. was supported by a fellowship from PAC (Progetto Strategico Regionale Calabria Alta Formazione) Calabria 2014/2020—Asse Prioritario 12, Linea B, Azione 10.5.12. C.R. acknowledges the support by a grant from the Italian Ministry of Health (Ricerca Corrente 2021). J.C. was supported by Italian Minister of University and Research [MIUR, D.M. 1062 del 10.08.2021]-PON R&I 2014–2020 "Azione IV.6 "Contratti di ricerca su tematiche Green" 1062_R13_GREEN. M.S.S. was supported by PON "R&I" 2014–2020—project from Area di Specializzazione "Salute", ARS01_00568 titled "SI.F.I.PA.CRO.DE.—Sviluppo e industrializzazione farmaci innovativi per terapia molecolare personalizzata PA. CRO. DE. for providing lab tools. GCV is supported by a fellow from the Italian Ministry of Health (5x1000 2018–2019).

Institutional Review Board Statement: Not applicable.

Informed Consent Statement: Not applicable.

Data Availability Statement: Not applicable.

Conflicts of Interest: The authors declare no conflict of interest.

References

1. Pucci, C.; Martinelli, C.; Ciofani, G. Innovative approaches for cancer treatment: Current perspectives and new challenges. *Ecancermedicalscience* **2019**, *13*, 961. [CrossRef] [PubMed]
2. Makhoba, X.H.; Viegas, C., Jr.; Mosa, R.A.; Viegas, F.P.D.; Pooe, O.J. Potential impact of the multi-target drug approach in the treatment of some complex diseases. *Drug Des. Dev. Ther.* **2020**, *14*, 3235–3249.
3. Han-Chung, W.; Chang, D.-K.; Chia-Ting, H. Targeted therapy for cancer. *J. Cancer Mol.* **2006**, *2*, 57–66.
4. Lee, Y.T.; Tan, Y.J.; Oon, C.E. Molecular targeted therapy: Treating cancer with specificity. *Eur. J. Pharmacol.* **2018**, *834*, 188–196. [CrossRef]
5. Malone, E.R.; Oliva, M.; Sabatini, P.J.B.; Stockley, T.L.; Siu, L.L. Molecular profiling for precision cancer therapies. *Genome Med.* **2020**, *12*, 8. [CrossRef]
6. Ouyang, L.; Luo, Y.; Tian, M.; Zhang, S.Y.; Lu, R.; Wang, J.H.; Kasimu, R.; Li, X. Plant natural products: From traditional compounds to new emerging drugs in cancer therapy. *Cell Prolif.* **2014**, *47*, 506–515. [CrossRef]
7. Lin, S.-R.; Chang, C.-H.; Hsu, C.-F.; Tsai, M.-J.; Cheng, H.; Leong, M.K.; Sung, P.-J.; Chen, J.-C.; Weng, C.-F. Natural compounds as potential adjuvants to cancer therapy: Preclinical evidence. *Br. J. Pharmacol.* **2020**, *177*, 1409–1423. [CrossRef]
8. Kumar, S.; Chang, Y.C.; Lai, K.H.; Hwang, T.L. Resveratrol, a molecule with anti-inflammatory and anti-cancer activities: Natural product to chemical synthesis. *Curr. Med. Chem.* **2021**, *28*, 3773–3786. [CrossRef]
9. Ko, J.-H.; Sethi, G.; Um, J.-Y.; Shanmugam, M.K.; Arfuso, F.; Kumar, A.P.; Bishayee, A.; Ahn, K.S. The role of resveratrol in cancer therapy. *Int. J. Mol. Sci.* **2017**, *18*, 2589. [CrossRef]
10. Chimento, A.; Santarsiero, A.; Iacopetta, D.; Ceramella, J.; De Luca, A.; Infantino, V.; Parisi, O.I.; Avena, P.; Bonomo, M.G.; Saturnino, C.; et al. A phenylacetamide resveratrol derivative exerts inhibitory effects on breast cancer cell growth. *Int. J. Mol. Sci.* **2021**, *22*, 5255. [CrossRef]
11. Chimento, A.; Sala, M.; Gomez-Monterrey, I.M.; Musella, S.; Bertamino, A.; Caruso, A.; Sinicropi, M.S.; Sirianni, R.; Puoci, F.; Parisi, O.I.; et al. Biological activity of 3-chloro-azetidin-2-one derivatives having interesting antiproliferative activity on human breast cancer cell lines. *Bioorg. Med. Chem. Lett.* **2013**, *23*, 6401–6405. [CrossRef] [PubMed]
12. Sala, M.; Chimento, A.; Saturnino, C.; Gomez-Monterrey, I.M.; Musella, S.; Bertamino, A.; Milite, C.; Sinicropi, M.S.; Caruso, A.; Sirianni, R.; et al. Synthesis and cytotoxic activity evaluation of 2,3-thiazolidin-4-one derivatives on human breast cancer cell lines. *Bioorg. Med. Chem. Lett.* **2013**, *23*, 4990–4995. [CrossRef]
13. Chimento, A.; Sirianni, R.; Saturnino, C.; Caruso, A.; Sinicropi, M.S.; Pezzi, V. Resveratrol and Its Analogs As Antitumoral Agents For Breast Cancer Treatment. *Mini Rev. Med. Chem.* **2016**, *16*, 699–709. [CrossRef] [PubMed]

14. Iacopetta, D.; Lappano, R.; Mariconda, A.; Ceramella, J.; Sinicropi, M.S.; Saturnino, C.; Talia, M.; Cirillo, F.; Martinelli, F.; Puoci, F.; et al. Newly synthesized imino-derivatives analogues of resveratrol exert inhibitory effects in breast tumor cells. *Int. J. Mol. Sci.* **2020**, *21*, 7797. [CrossRef] [PubMed]
15. Urbani, P.; Ramunno, A.; Filosa, R.; Pinto, A.; Popolo, A.; Bianchino, E.; Piotto, S.; Saturnino, C.; De Prisco, R.; Nicolaus, B.; et al. Antioxidant activity of diphenylpropionamide derivatives: Synthesis, biological evaluation and computational analysis. *Molecules* **2008**, *13*, 749–761. [CrossRef]
16. Guo, K.; Feng, Y.; Zheng, X.; Sun, L.; Wasan, H.S.; Ruan, S.; Shen, M. Resveratrol and Its Analogs: Potent Agents to Reverse Epithelial-to-Mesenchymal Transition in Tumors. *Front. Oncol.* **2021**, *11*, 644134. [CrossRef]
17. Yilmaz, M.; Christofori, G. EMT, the cytoskeleton, and cancer cell invasion. *Cancer Metastasis Rev* **2009**, *28*, 15–33. [CrossRef]
18. Fujiwara, I.; Zweifel, M.E.; Courtemanche, N.; Pollard, T.D. Latrunculin A accelerates actin filament depolymerization in addition to sequestering actin monomers. *Curr. Biol.* **2018**, *28*, 3183–3192.e3182. [CrossRef]
19. Rebowski, G.; Boczkowska, M.; Drazic, A.; Ree, R.; Goris, M.; Arnesen, T.; Dominguez, R. Mechanism of actin N-terminal acetylation. *Sci. Adv.* **2020**, *6*, 8793. [CrossRef]
20. Morris, G.M.; Huey, R.; Lindstrom, W.; Sanner, M.F.; Belew, R.K.; Goodsell, D.S.; Olson, A.J. AutoDock4 and AutoDockTools4: Automated docking with selective receptor flexibility. *J. Comput. Chem.* **2009**, *30*, 2785–2791. [CrossRef]
21. Cesarini, S.; Spallarossa, A.; Ranise, A.; Schenone, S.; Rosano, C.; La Colla, P.; Sanna, G.; Busonera, B.; Loddo, R. N-Acylated and N,N′-diacylated imidazolidine-2-thione derivatives and N,N′-diacylated tetrahydropyrimidine-2(1H)-thione analogues: Synthesis and antiproliferative activity. *Eur. J. Med. Chem.* **2009**, *44*, 1106–1118. [CrossRef] [PubMed]
22. Rosano, C.; Lappano, R.; Santolla, M.F.; Ponassi, M.; Donadini, A.; Maggiolini, M. Recent advances in the rationale design of GPER ligands. *Curr. Med. Chem.* **2012**, *19*, 6199–6206. [CrossRef] [PubMed]
23. Santolla, M.F.; De Francesco, E.M.; Lappano, R.; Rosano, C.; Abonante, S.; Maggiolini, M. Niacin activates the G protein estrogen receptor (GPER)-mediated signalling. *Cell Signal* **2014**, *26*, 1466–1475. [CrossRef] [PubMed]
24. Sanner, M.F.; Duncan, B.S.; Carrillo, C.J.; Olson, A.J. Integrating computation and visualization for biomolecular analysis: An example using python and AVS. In Proceedings of the Pacific Symposium on Biocomputing 1999, Mauna Lani, HI, USA, 4–9 January 1999; pp. 401–412.
25. Viale, M.; Cordazzo, C.; De Totero, D.; Budriesi, R.; Rosano, C.; Leoni, A.; Ioan, P.; Aiello, C.; Croce, M.; Andreani, A.; et al. Inhibition of MDR1 activity and induction of apoptosis by analogues of nifedipine and diltiazem: An in vitro analysis. *Investig. New Drugs* **2011**, *29*, 98–109. [CrossRef]
26. Pettersen, E.F.; Goddard, T.D.; Huang, C.C.; Couch, G.S.; Greenblatt, D.M.; Meng, E.C.; Ferrin, T.E. UCSF Chimera—A visualization system for exploratory research and analysis. *J. Comput. Chem.* **2004**, *25*, 1605–1612. [CrossRef]
27. Iacopetta, D.; Rosano, C.; Sirignano, M.; Mariconda, A.; Ceramella, J.; Ponassi, M.; Saturnino, C.; Sinicropi, M.S.; Longo, P. Is the way to fight cancer paved with gold? Metal-based carbene complexes with multiple and fascinating biological features. *Pharmaceuticals* **2020**, *13*, 91. [CrossRef]
28. Iacopetta, D.; Ceramella, J.; Rosano, C.; Mariconda, A.; Pellegrino, M.; Sirignano, M.; Saturnino, C.; Catalano, A.; Aquaro, S.; Longo, P.; et al. N-Heterocyclic Carbene-Gold(I) complexes targeting actin polymerization. *Appl. Sci.* **2021**, *11*, 5626. [CrossRef]
29. Pijuan, J.; Barceló, C.; Moreno, D.F.; Maiques, O.; Sisó, P.; Marti, R.M.; Macià, A.; Panosa, A. In vitro cell migration, invasion, and adhesion assays: From cell imaging to data analysis. *Front. Cell Dev. Biol.* **2019**, *7*, 107. [CrossRef]
30. Iacopetta, D.; Carocci, A.; Sinicropi, M.S.; Catalano, A.; Lentini, G.; Ceramella, J.; Curcio, R.; Caroleo, M.C. Old drug scaffold, new activity: Thalidomide-correlated compounds exert different effects on breast cancer cell growth and progression. *Chem. Med. Chem.* **2017**, *12*, 381–389. [CrossRef]
31. Shaw, F.L.; Harrison, H.; Spence, K.; Ablett, M.P.; Simões, B.M.; Farnie, G.; Clarke, R.B. A detailed mammosphere assay protocol for the quantification of breast stem cell activity. *J. Mammary Gland. Biol. Neoplasia* **2012**, *17*, 111–117. [CrossRef]
32. De Luca, A.; Fiorillo, M.; Peiris-Pagès, M.; Ozsvari, B.; Smith, D.L.; Sanchez-Alvarez, R.; Martinez-Outschoorn, U.E.; Cappello, A.R.; Pezzi, V.; Lisanti, M.P.; et al. Mitochondrial biogenesis is required for the anchorage-independent survival and propagation of stem-like cancer cells. *Oncotarget* **2015**, *6*, 14777–14795. [CrossRef] [PubMed]
33. Saturnino, C.; Barone, I.; Iacopetta, D.; Mariconda, A.; Sinicropi, M.S.; Rosano, C.; Campana, A.; Catalano, S.; Longo, P.; Andò, S. N-heterocyclic carbene complexes of silver and gold as novel tools against breast cancer progression. *Future Med. Chem.* **2016**, *8*, 2213–2229. [CrossRef] [PubMed]
34. Sinicropi, M.S.; Lappano, R.; Caruso, A.; Santolla, M.F.; Pisano, A.; Rosano, C.; Capasso, A.; Panno, A.; Lancelot, J.C.; Rault, S.; et al. (6-bromo-1,4-dimethyl-9H-carbazol-3-yl-methylene)-hydrazine (carbhydraz) acts as a GPER agonist in breast cancer cells. *Curr. Top. Med. Chem.* **2015**, *15*, 1035–1042. [CrossRef]
35. Stec-Martyna, E.; Ponassi, M.; Miele, M.; Parodi, S.; Felli, L.; Rosano, C. Structural comparison of the interaction of tubulin with various ligands affecting microtubule dynamics. *Curr. Cancer Drug Targets* **2012**, *12*, 658–666. [CrossRef] [PubMed]
36. Grintsevich, E.E.; Ahmed, G.; Ginosyan, A.A.; Wu, H.; Rich, S.K.; Reisler, E.; Terman, J.R. Profilin and Mical combine to impair F-actin assembly and promote disassembly and remodeling. *Nat. Commun.* **2021**, *12*, 5542. [CrossRef]
37. Steinmetz, M.O.; Prota, A.E. Microtubule-targeting agents: Strategies to hijack the cytoskeleton. *Trends Cell. Biol.* **2018**, *28*, 776–792. [CrossRef]
38. Thomas, E.; Gopalakrishnan, V.; Hegde, M.; Kumar, S.; Karki, S.S.; Raghavan, S.C.; Choudhary, B. A novel resveratrol based tubulin inhibitor induces mitotic arrest and activates apoptosis in cancer cells. *Sci. Rep.* **2016**, *6*, 1–13. [CrossRef]

39. Schneider, Y.; Chabert, P.; Stutzmann, J.; Coelho, D.; Fougerousse, A.; Gosse, F.; Launay, J.F.; Brouillard, R.; Raul, F. Resveratrol analog (Z)-3,5,4′-trimethoxystilbene is a potent anti-mitotic drug inhibiting tubulin polymerization. *Int. J. Cancer* **2003**, *107*, 189–196. [CrossRef]
40. Yin, Y.; Lian, B.P.; Xia, Y.Z.; Shao, Y.Y.; Kong, L.Y. Design, synthesis and biological evaluation of resveratrol-cinnamoyl derivates as tubulin polymerization inhibitors targeting the colchicine binding site. *Bioorg. Chem.* **2019**, *93*, 103319. [CrossRef]
41. Jiang, P.; Enomoto, A.; Takahashi, M. Cell biology of the movement of breast cancer cells: Intracellular signalling and the actin cytoskeleton. *Cancer Lett.* **2009**, *284*, 122–130. [CrossRef]
42. Bravo-Cordero, J.J.; Hodgson, L.; Condeelis, J. Directed cell invasion and migration during metastasis. *Curr. Opin. Cell Biol.* **2012**, *24*, 277–283. [CrossRef] [PubMed]
43. Pinto, B.; Henriques, A.C.; Silva, P.M.A.; Bousbaa, H. Three-dimensional spheroids as in vitro preclinical models for cancer research. *Pharmaceutics* **2020**, *12*, 1186. [CrossRef] [PubMed]
44. Weiswald, L.B.; Bellet, D.; Dangles-Marie, V. Spherical cancer models in tumor biology. *Neoplasia* **2015**, *17*, 1–15. [CrossRef]
45. Nath, S.; Devi, G.R. Three-dimensional culture systems in cancer research: Focus on tumor spheroid model. *Pharmacol. Ther.* **2016**, *163*, 94–108. [CrossRef]
46. Trepat, X.; Chen, Z.; Jacobson, K. Cell migration. *Compr. Physiol.* **2012**, *2*, 2369–2392.
47. Iacopetta, D.; Carrisi, C.; De Filippis, G.; Calcagnile, V.M.; Cappello, A.R.; Chimento, A.; Curcio, R.; Santoro, A.; Vozza, A.; Dolce, V.; et al. The biochemical properties of the mitochondrial thiamine pyrophosphate carrier from Drosophila melanogaster. *FEBS J.* **2010**, *277*, 1172–1181. [CrossRef] [PubMed]
48. Yang, Y.; Zheng, H.; Zhan, Y.; Fan, S. An emerging tumor invasion mechanism about the collective cell migration. *Am. J. Transl. Res.* **2019**, *11*, 5301–5312. [PubMed]